C_3N_4 anchored ZIF 8 composites: Photo-regenerable, high capacity sorbents as adsorptive photocatalysts for the effective removal of tetracycline from water

Suyana Panneri [a] [b], Minju Thomas [a] [b], Priyanka Ganguly [a], Balagopal N. Nair [c] [d], Abdul Azeez Peer Mohamed [a] , K.G.K. Warrier [a] and U. S. Hareesh *[a] [b]

[a]Materials Science and Technology Division, National Institute for Interdisciplinary Science and Technology (CSIR-NIIST), Thiruvananthapuram - 695019, India
[b]Academy of Scientific and Innovative Research (AcSIR), New Delhi, India
[c]R&D Center, Noritake Co. Limited, Aichi 470-0293, Japan
[d]Nanochemistry Research Institute , Department of Chemistry, Curtin University, GPO Box UI987, Perth, WA 6845, Australia

Table S1: Reported works on ZIF-8 based composite photocatalysts

ZIF-8 based composites with other semiconductor				
Sample Name	Semiconductor	MOF	Application	Ref
Pt/ZIF-8 loaded TiO_2 nanotubes	TiO_2	ZIF-8	Phenol degradation	1
ZIF-8/Zn_2GeO_4	Zn_2GeO_4	ZIF-8	CO_2 conversion to CH_3OH	2
Ag/AgCl@ZIF-8	Ag/AgCl	ZIF-8	Rhodamine B degradation	3
TiO_2@ZIF-8	TiO_2	ZIF-8	Rhodamine B and methylene blue degradation	4
TiO_2/ZIF-8	TiO_2	ZIF-8	Rhodamine B degradation	
ZnO@ZIF‑8	ZnO	ZIF-8	Cr and Methylene blue degradation	5

Table S2: Reported works on C_3N_4 based composite photocatalysts

C_3N_4 based composites with other MOF				
Sample Name	Semiconductor	MOF	Application	Ref
UiO-66/ g-C_3N_4	g-C_3N_4	UiO-66	Photocatalytic H_2 production	6
C_3N_4/MIL-100(Fe)	g-C_3N_4	MIL100 (Fe)	Rhodamine B degradation	7
C_3N_4/MIL-125(Ti)	g-C_3N_4	MIL-125(Ti)	Rhodamine B degradation	8

Table S3. Different compositions of C_3N_4-ZIF-8

Sl No	Sample	Wt % of C_3N_4	Wt % of ZIF-8
1	ZC0	30	70
2	ZC	60	40
3	ZC1	95	5

Characterization of materials

Composition and thermal stability of the prepared photocatalysts were analyzed by thermogravimetric analysis (Perkin Elmer STA 6000, USA) in the temperature range of 50-800 ° C at a heating rate of 5° C/ min in the air atmosphere. The crystal structure and phase purity of the prepared samples were obtained by X-ray diffraction (XRD) using a Philips X'pert Pro diffractometer in the 2θ range of 5-70° using Cu Kα radiation. X-ray photoelectron spectroscopy (XPS) was done on an ESCA + Omicron nanotechnology (Oxford instrument, Germany) spectrometer equipped with a Mg Kα X-ray source (hυ = 1253.6 eV). Morphology and microstructure of the prepared samples were investigated by high-resolution transmission electron microscope (HETEM, Technai G^2, FEI, and The Netherlands) at an accelerating voltage of 300 KV. The elemental composition of the samples was studied using energy dispersive spectrum (EDS) attached to the transmission electron microscope. The SEM micrographs were obtained from scanning electron microscope made by Carl Zeiss, Germany.

The Brunauer- Emmett- Teller (BET) surface area measurements were done by nitrogen adsorption (Micromeritics Tristar 2 USA surface area and porosity analyzer) after degassing at 200° C for 2 hrs. The UV- Visible absorption spectra of the prepared samples were recorded by a Shimadzu UV 2401 PC spectrophotometer in the range of 200- 800 nm and emission spectra were obtained from a spectrofluorometer (Cary Eclipse, Varian, The Netherlands). The prepared materials were also investigated by Fourier Transform Infrared (FT-IR) spectra using a Bruker FT-IR spectrometer for functional group identification. The photoluminescence spectrum was measured using a spectrofluorometer (Cary Eclipse, Varian, Netherlands). The photocatalytic degradations of tetracycline ((TC) were monitored by a UV-visible spectrometer (UV 2401 PC, Shimadzu, Japan) at different time intervals. The zeta potential of the samples was measured by a Zeta potential analyzer (Zetasizer Nano zs90) at different pH values.

Adsorption capacity, isotherm, and kinetics of ZC using TC

The adsorption capacity, isotherm, and kinetics of ZC were predicted using 50-400 μM TC solution. 100 mg/L of photocatalyst was added in different TC concentration and stirred in dark for 60 min. Samples were collected after a regular time interval and the change in TC concentration was measured at 357 nm using a UV-Vis spectrophotometer. The concentration of surface adsorbed TC was calculated using the equation of form;

$$\%TC\ adsorbed = \left(\frac{C_0 - C_t}{C_0}\right) \times 100 \qquad \text{Equation (S1)}$$

where $\mathbf{C_0}$ (mg L^{-1}) and $\mathbf{C_t}$ (mg L^{-1}) correspond to the TC concentration at the start and after contact time **t** (min).

The adsorption capacity of the composite was investigated by subjecting them in varying concentration of TC solutions (50 -400 μm). The adsorption capacity, $\mathbf{q_e}$ (mg g^{-1}), of TC solution retained per gram of adsorbent at the equilibrium concentration ($\mathbf{C_e}$) was calculated using the equation;

$$q_e = \frac{(C_0 - C_e)}{m} \times V \qquad \text{Equation (S2)}$$

Where $\mathbf{C_0}$ and $\mathbf{C_e}$ are the initial and equilibrium concentrations of TC in aqueous solution, **V** is the solution volume and **m** is the amount of adsorbent added.

The adsorption data of 200 μM TC was evaluated using the isotherm models of Langmuir, Freundlich, and Dubinin–Kaganer–Radushkevich (DKR).

Linear form of the Freundlich isotherm model

$$lnq_e = \left(\frac{1}{n}\right) lnC_e + lnK_f \qquad \text{Equation (S3)}$$

Where K_f ($mg^{1-1/n}\ g^{-1}\ L^{1/n}$) is the Freundlich constant related to the Gibb's free energy of adsorption and n (gL^{-1}) is another Freundlich constant related to the adsorption intensity.

Langmuir isotherm model is;

$$\frac{C_e}{q_e} = \frac{1}{q_m} C_e + \frac{1}{q_m \times K_l} \qquad \text{Equation (S4)}$$

Where $\mathbf{q_m}$ is the adsorption intensity and $\mathbf{K_L}$ is Langmuir constant.

DKR model is;

$$lnq_e = lnq_m - \beta\varepsilon^2 \qquad \text{Equation (S5)}$$

Where **β** ($mol^2\ J^{-2}$) is constant related to adsorption energy and **ε** is Polanyi potential.

The rate at which the TC is adsorbed from an aqueous solution of the ZC composite is analyzed using different kinetic models. The adsorption data of 100 μM TC fits the pseudo-second order kinetics which can be represented as

$$\frac{t}{q_t} = \left(\frac{1}{q_e}\right) \times t + \frac{1}{K_2 \times q_e^2}$$ Equation (S6)

where K_2 (g mg^{-1} min^{-1}) is pseudo-second order rate constants and q_t is the amount of TC adsorbed on the surface per unit mass of adsorbent (mg g^{-1}) at the contact time of t.

Effect of pH and zeta potential

The effect of pH on adsorption of TC solution (200 μM) by ZC composite at different pH ranging from 2-12 was estimated using dilute HCl and NaOH solution. The adsorption experiments were conducted in dark for 60 min and the change in TC concentration was measured at 357 nm using a UV-Vis spectrophotometer. To study the effect of zeta potential on the adsorption of TC using ZC composite was studied. The surface charge of ZC solutions at different pH ranging from 2-12 was estimated.

Reusability of ZC

5 cyclic runs were conducted to check the stability of the prepared bifunctional (adsorption cum photocatalysis) catalyst. In a typical experiment, a weighed amount of catalyst was added in 200 μM TC solution and subjected to adsorption in the dark followed by sunlight-induced photocatalysis. The powder retained was washed with deionized water, dried and used as such for further cyclic runs.

Active species trapping

To ascertain the reactive oxidative species generated in the photocatalytic degradation system, the species trapping experiments were conducted. In a typical experiment 10mM of Isopropanol (IPA) (as a quencher of $OH^-)\cdot$, 6mM $AgNO_3$ (as a quencher of an electron), 6mM Benzoquinone (BQ) (as a quencher of O_2^-) and 10mM Triethanolamine (TEA) (as a quencher of holes) were respectively added in the photocatalytic system and irradiated under sunlight. The change in TC concentration at 357 nm was investigated using a UV-Vis spectrophotometer.

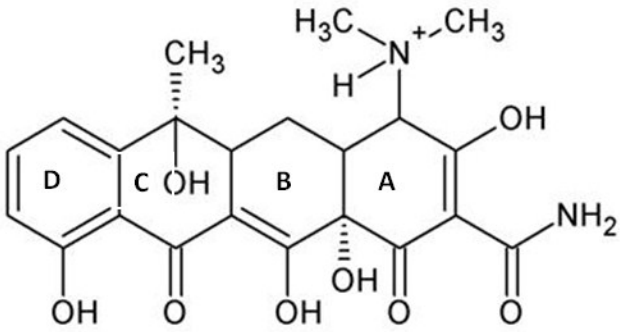

Fig. S1 Tetracycline (TC) molecule

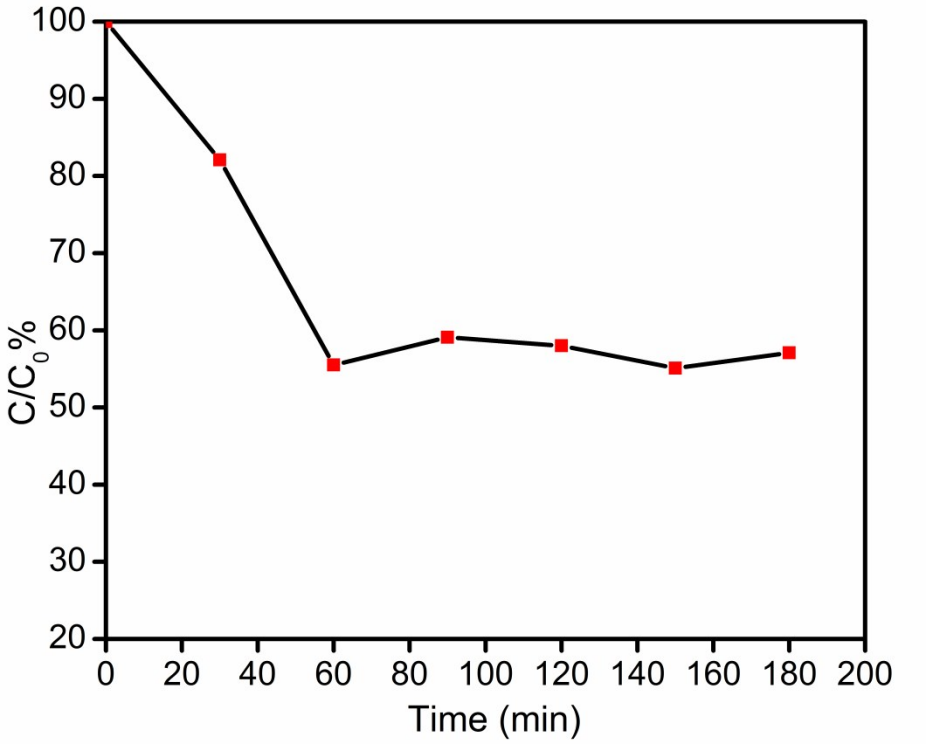

Fig. S2 Adsorption of TC using C_3N_4-ZIF-8 (ZC) composite in dark

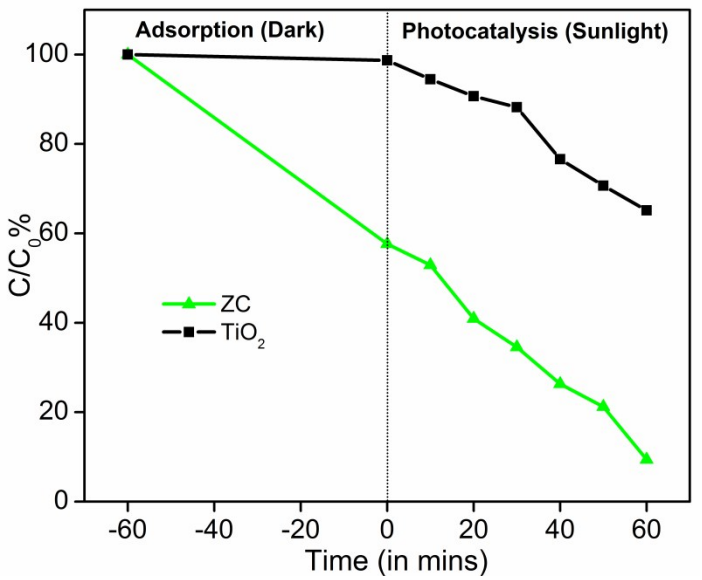

Fig. S3 Photocatalytic degradation profile of TC using ZC and Degussa TiO_2

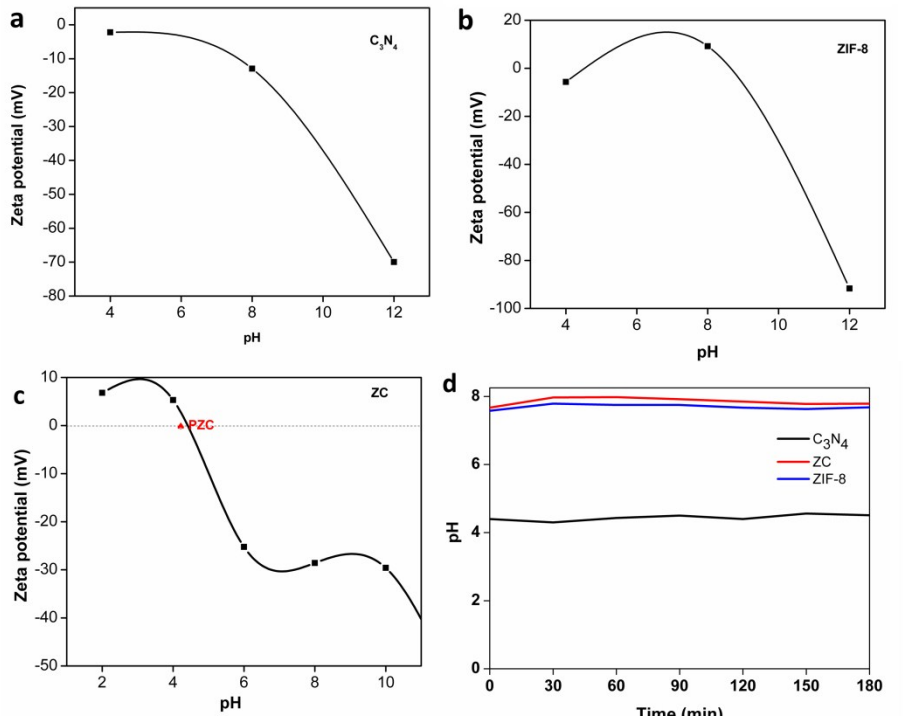

Fig. S4 Zeta potential curves of a) C_3N_4 b) ZIF-8 and c) ZC; d) the pH values with time of all the three samples in 200 micromolar aqueous TC solution

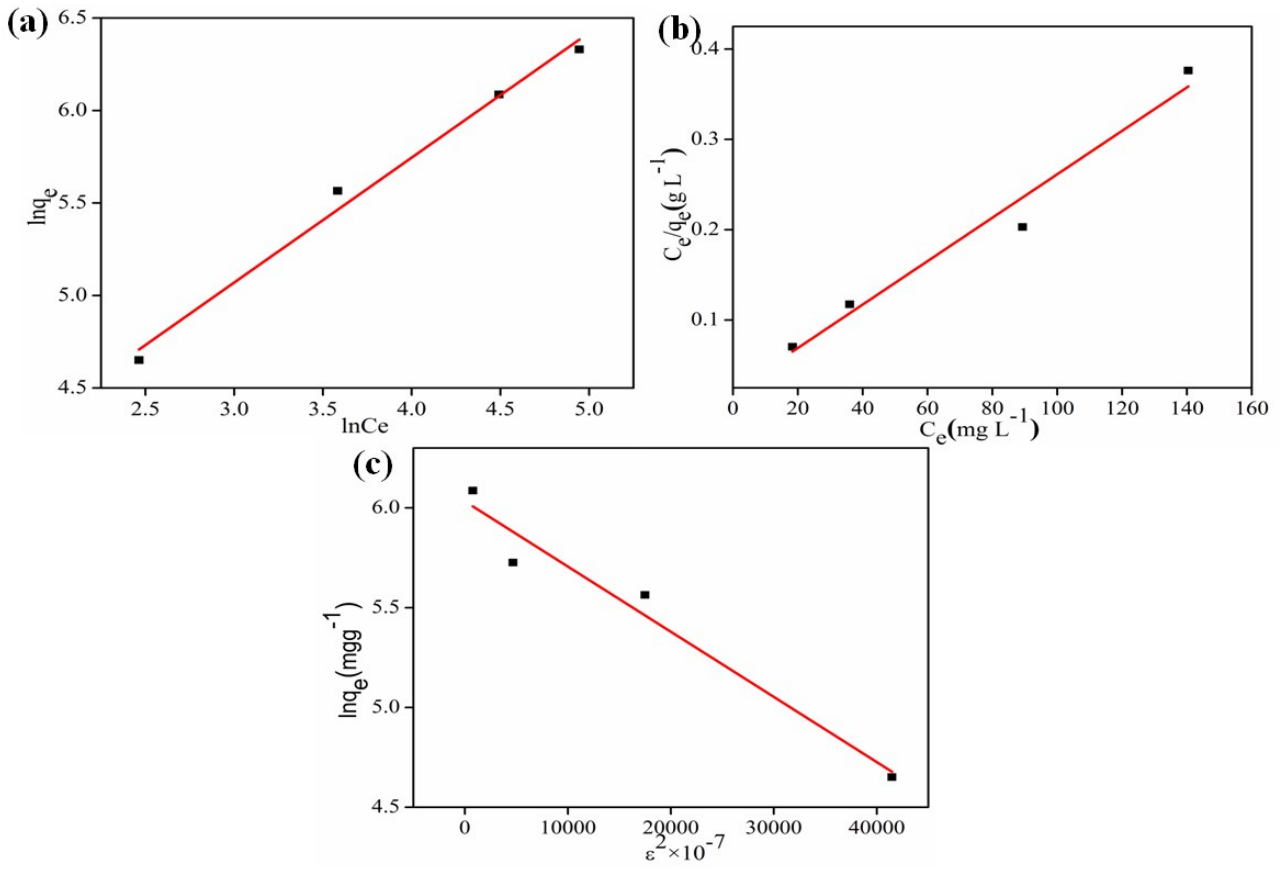

Fig. S5 (a) Freundlich, (b) Langmuir and (c) Dubinin–Kaganer–Radushkevich (DKR) adsorption isotherms of 200 μM TC adsorption

Table S4. Summary of the parameters related to Freundlich isotherm

Concentration	200 μM
Isotherm	Freundlich isotherm
R^2	0.999
1/n	0.675

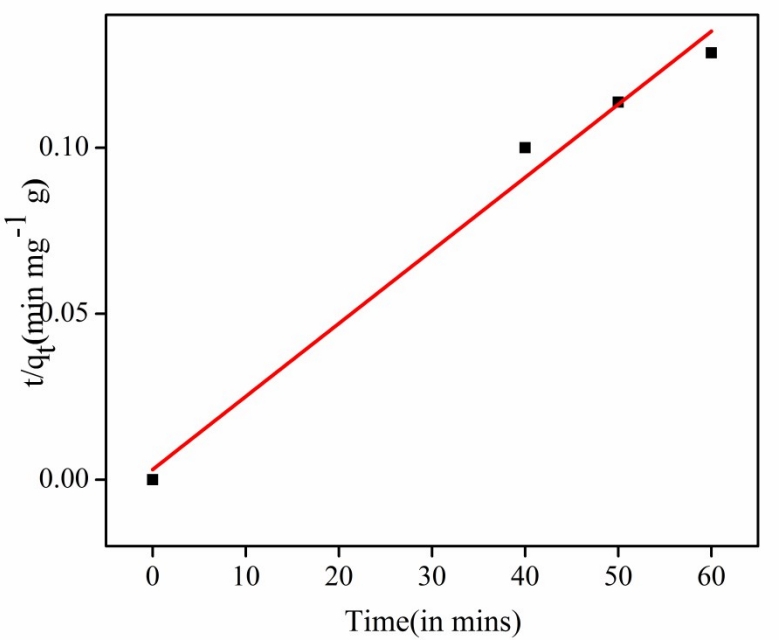

Fig. S6 Pseudo-second order kinetics of 200 µM TC adsorption

Table S5: Summary of the parameters related to pseudo-second order kinetics

Concentration	100 µM
Kinetics	Pseudo-second order
R^2	0.989
K_2	0.0013
q_e (calculated)	500
q_e (experimental)	420

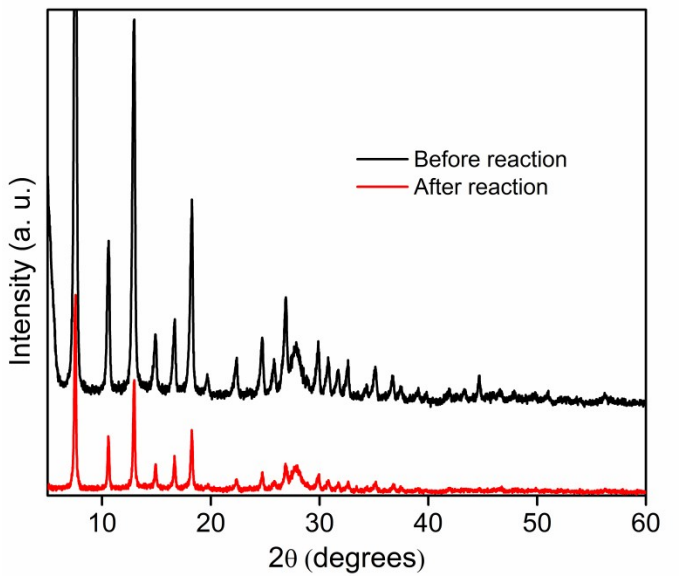

Fig. S7 XRD pattern of ZC before and after photocatalytic reactions

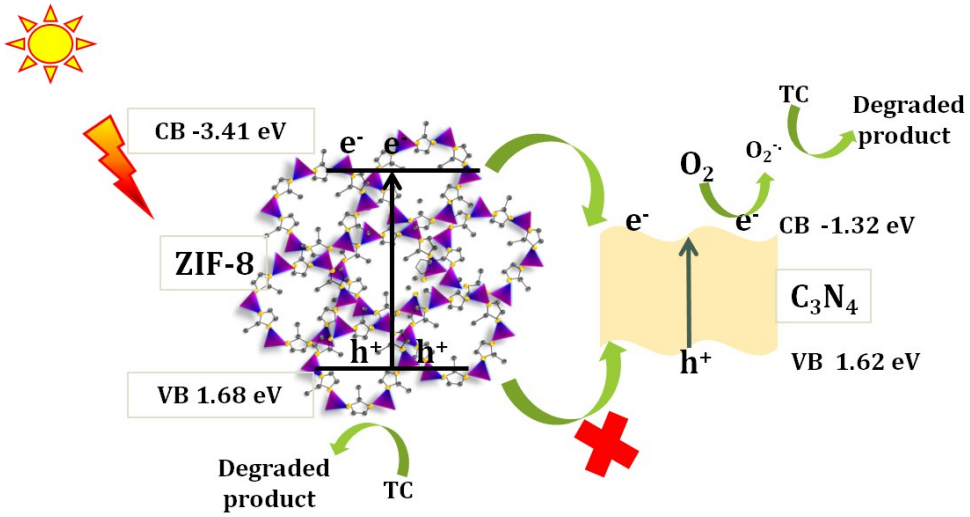

Fig. S8 Photocatalytic degradation of TC by ZC composite through the formation of Type I heterostructure

References

1. Isimjan, T. T.; Kazemian, H.; Rohani, S.; Ray, A. K., Photocatalytic activities of Pt/ZIF-8 loaded highly ordered TiO2 nanotubes. *J. Mater. Chem.* **2010,** *20* (45), 10241-10245.

2. Liu, Q.; Low, Z.-X.; Li, L.; Razmjou, A.; Wang, K.; Yao, J.; Wang, H., ZIF-8/Zn2GeO4 nanorods with an enhanced CO2 adsorption property in an aqueous medium for photocatalytic synthesis of liquid fuel. *Journal of Materials Chemistry A* **2013,** *1* (38), 11563-11569.

3. Gao, S.-T.; Liu, W.-H.; Shang, N.-Z.; Feng, C.; Wu, Q.-H.; Wang, Z.; Wang, C., Integration of a plasmonic semiconductor with a metal-organic framework: a case of Ag/AgCl@ZIF-8 with enhanced visible light photocatalytic activity. *RSC Advances* **2014,** *4* (106), 61736-61742.
4. Chandra, R.; Mukhopadhyay, S.; Nath, M., TiO2@ZIF-8: A novel approach of modifying micro-environment for enhanced photo-catalytic dye degradation and high usability of TiO2 nanoparticles. *Mater. Lett.* **2016,** *164*, 571-574.
5. Zeng, X.; Huang, L.; Wang, C.; Wang, J.; Li, J.; Luo, X., Sonocrystallization of ZIF-8 on Electrostatic Spinning TiO2 Nanofibers Surface with Enhanced Photocatalysis Property through Synergistic Effect. *ACS Applied Materials & Interfaces* **2016,** *8* (31), 20274-20282.
6. Wang, R.; Gu, L.; Zhou, J.; Liu, X.; Teng, F.; Li, C.; Shen, Y.; Yuan, Y., Quasi-Polymeric Metal–Organic Framework UiO-66/g-C3N4 Heterojunctions for Enhanced Photocatalytic Hydrogen Evolution under Visible Light Irradiation. *Advanced Materials Interfaces* **2015,** *2* (10), n/a-n/a.
7. Hong, J.; Chen, C.; Bedoya, F. E.; Kelsall, G. H.; O'Hare, D.; Petit, C., Carbon nitride nanosheet/metal-organic framework nanocomposites with synergistic photocatalytic activities. *Catalysis Science & Technology* **2016,** *6* (13), 5042-5051.
8. Wang, H.; Yuan, X.; Wu, Y.; Zeng, G.; Chen, X.; Leng, L.; Li, H., Synthesis and applications of novel graphitic carbon nitride/metal-organic frameworks mesoporous photocatalyst for dyes removal. *Applied Catalysis B: Environmental* **2015,** *174–175*, 445-454.